A LOCAL POST-PROCESSING APPROACH FOR FORCE COMPUTATION IN TUBULAR MOTORS

H. De Gersem, K. Hameyer

Katholieke Universiteit Leuven, Dep. EE (ESAT), Div. ELEN,
Kardinaal Mercierlaan 94, B-3001 Leuven, Belgium
Fax +32-16-321985; e-mail: Herbert.DeGersem@esat.kuleuven.ac.be

Abstract: Deriving the magnetic force in moving devices from a finite element solution is troublesome because of the numerical differentiation applied to the magnetic vector potential to obtain the magnetic flux density. A higher accuracy is achieved by performing a local analytic post-processing step applied to the air gap region between the moving bodies. For axisymmetric models, a finite Fourier-Bessel series serves as the approximative local analytic solution for the potential field. Differentiation and integration is performed analytically on the series. Applying the Maxwell stress method to the local solution results in a force computation scheme that keeps the same convergence rate as the potential field solution. This enhanced method is applied to a tubular switched reluctance actuator. A comparison is set up between the classical Maxwell stress method and the new approach.

1.- INTRODUCTION

The design and optimisation of electric devices employ numerical simulation. In the case of finite element models, the accuracy of the simulation and the problem size are two factors that have to be balanced in order to obtain a good trade-off between accuracy and computational efforts. The problem size is mainly determined by the number of degrees of freedom in the finite element model. The accuracy of the computation depends on the tolerances of the material data and geometry, the truncation errors due to the finite element discretisation and the error propagation in all pre- and post-processing routines. The calculation of forces is responsible for a significant part of the error propagation. It requires a field solution that is far more accurate than the resulting force is. The aim of this paper is to develop a method that keeps this error propagation as small as possible during the post-process.

2.- AXISYMMETRIC MAGNETOSTATIC FORMULATION

The choice of the magnetic vector potential $\mathbf{A}$ with $\mathbf{B} = \nabla \times \mathbf{A}$ fulfills the divergence-free condition for the magnetic flux density $\mathbf{B}$. In the magnetostatic case, Ampère's law yields the partial differential equation

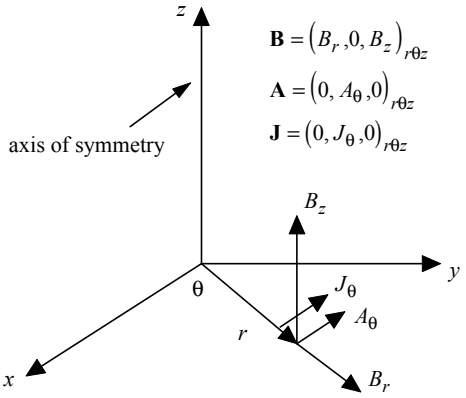

Fig. 1. r θ z and xyz coordinate systems.

$$\nabla \times (\nu \nabla \times \mathbf{A}) = \mathbf{J}\,, \tag{1}$$

where ν is the magnetic reluctivity and $\mathbf{J}$ the imposed current density.

A lot of electromagnetic devices, e.g. actuators with a cylindrical plunger and tubular motors, have mainly a cylindrical geometry and are excited by cylindrical windings. Their behaviour can be computed using an axisymmetric model with cylindrical boundary conditions and imposed currents in the tangential direction. The magnetic flux appears in the (r,z)-plane whereas the magnetic vector potential has only a component in the θ-direction (fig. 1). Equation (1) is reduced to [1],[2]

$$\frac{\partial}{\partial r}\left(\frac{\nu}{r}\frac{\partial (rA_\theta)}{\partial r}\right) + \frac{\partial}{\partial z}\left(\nu \frac{\partial A_\theta}{\partial z}\right) = -J_\theta\,. \tag{2}$$

Obtaining an accurate solution in the neighbourhood of the axis of symmetry requires special treatment of the elements close to this axis, the use of higher order elements or the choice of special potentials [3]. Here, the potential $\phi = rA_\theta$ is chosen. The integrals of hyperbolic terms are performed analytically for the elements close to the axis.

3.- DISCRETISATION ERROR

The global error ε of a 2D finite element solution is

$$\|\varepsilon\| \leq C \cdot h^{p}, \tag{3}$$

where h represents the characteristic mesh size, p denotes the asymptotic rate of convergence and C is the convergence factor [4]. The convergence rate expresses the exponential decay of the discretisation error according to the decreasing mesh size h. The convergence factor is an upper bound independent of the mesh size and is influenced by the aspect ratio of the elements, the accuracy of the numerical integration and rounding-off errors.

The asymptotic rate of convergence depends on the nature of the partial differential equation and the choice of base and test functions. In the case of elliptic partial differential equations, the error decays by

$$\|\varepsilon\| \leq C \cdot h^{q+1}, \tag{4}$$

where q denotes the polynomial order of the elements [4],[5]. Using first order elements, the rate of convergence is $O(h^2)$. In terms of the number of degrees of freedom (DOF), the convergence is of order $O(DOF^{-1})$.

Unfortunately, the convergence rate decreases by one when numerical differentiation is applied. As a consequence, the convergence rate of derived quantities such as flux densities and forces is of the order $O(h^q)$, e.g. $O(h)$ for first order elements. This fact indicates the difficulty in obtaining accurate forces out of a finite element potential solution. Even when the error on the potential field reaches a desired limit, the force error is considerable higher.

4.- IMPROVING THE MAXWELL STRESS METHOD

The Maxwell stress method computes the force out of the magnetic flux density

$$\mathbf{B} = \left(B_r, 0, B_z\right) = \left(-\frac{\partial A_\theta}{\partial z}, 0, \frac{1}{r}\frac{\partial\left(rA_\theta\right)}{\partial r}\right). \tag{5}$$

$\mathbf{B}$ is derived from the finite element solution

$$A_\theta = \sum_j A_{\theta j} N_j \tag{6}$$

by differentiating the form functions N_j. The result of this approach depends on the chosen contour of integration and the local orientation of the mesh. It is known that considerable errors appear when the mesh at the place of evaluation is rough or when the contour passes the neighbourhood of sharp corners in the model. Several improvements and error estimates are proposed in literature [6],[7],[8]. The accuracy can be increased by choosing a denser mesh, higher order elements or a dual formulation [9], all at the expense of a larger problem size. A second approach tries to overcome local erratic effects by error cancellation techniques [10],[11] or local smoothing [12],[13], e.g. by averaging the forces obtained by integration along several contours. Thirdly, some implementations pay particular attention to the orientation of the mesh or to the choice of an optimal path for integration [8]. Although all improvements increase the accuracy, some of them still rely on numerical differentiation and consequently do not improve the rate of the convergence of the force error. This however is essential to guarantee the maximum accuracy from a given discretisation.

5.- SUPERCONVERGENCE AND LOCAL POST-PROCESSING

If the harmful numerical differentiation can be avoided, the force computation will retain the same convergence rate as the potential field. A method that converges at a higher convergence rate than predicted by the finite element theory, is called *superconvergent* [14]. Superconvergence can be achieved by local analytic post-processing operations [15]. Local post-processing has already been applied succesfully to calculate flux densities [15], energies and local forces acting on charged particles [16]. Computing forces using the Maxwell stress method combined with a local post-processing approach is presented for Cartesian 2D models in [17], [15] and [12] and for 3D models in [5]. In this paper, a local post-processing scheme is developed for force computation in axisymmetric models.

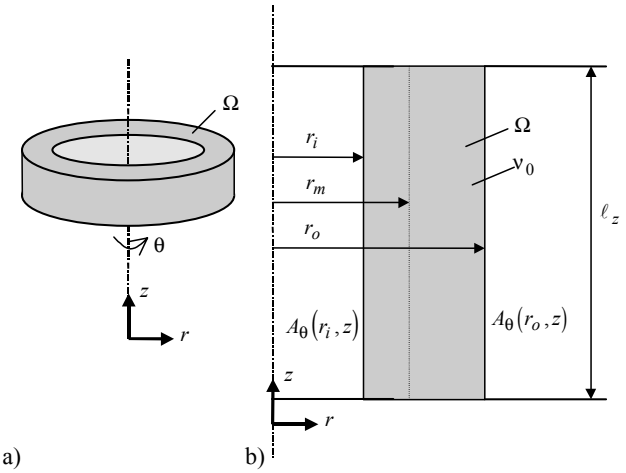

Fig. 2. a) Domain of the analytic post-processing step.
b) Cross-section of the post-processing domain.

6.- LOCAL ANALYTIC SOLUTION

Consider a domain with a rectangular section in the (r,z)-plane (fig. 2). Suppose that the values for the magnetic vector potential are known from a beforehand computed finite element solution evaluated on the boundaries $r = r_i$ and $r = r_o$. The magnetic field is assumed to be periodic in the z-direction:

$$\begin{cases} A_\theta(r_i, z) = f_i(z) \\ A_\theta(r_o, z) = f_o(z) \\ A_\theta(r, z + \ell_z) = A_\theta(r, z) \,. \end{cases} \tag{7}$$

The domain contains a homogeneous, isotropic and linear material. There are no imposed currents. The governing differential equation is

$$\frac{\partial}{\partial r}\left(\frac{1}{r}\frac{\partial(rA_\theta)}{\partial r}\right) + \frac{\partial^2 A_\theta}{\partial z^2} = 0 \,. \tag{8}$$

The analytic solution is found by the separation of the unknowns:

$$\begin{aligned} A_\theta = \sum_k & \left(\alpha_k \cos(\lambda_k z) + \beta_k \sin(\lambda_k z)\right) \\ & \cdot \left(\chi_k \, \mathrm{I}_1(\lambda_k r) + \delta_k \, \mathrm{K}_1(\lambda_k r)\right) \\ & + \left(\varepsilon_k \sinh(\lambda_k z) + \phi_k \cosh(\lambda_k z)\right) \\ & \cdot \left(\gamma_k \, \mathrm{J}_1(\lambda_k r) + \eta_k \, \mathrm{Y}_1(\lambda_k r)\right) \end{aligned} \tag{9}$$

where α_k, β_k, χ_k, δ_k, ε_k, ϕ_k, γ_k and η_k are unknown coefficients, J_p and Y_p are Bessel functions of order p and I_p and K_p are modified Bessel functions of order p [18],[19].

Because of the z-periodicity of the boundary conditions, the hyperbolic terms in (9) disappear and the possible spatial frequencies λ are of the form $\lambda_k = \dfrac{2\pi k}{\ell_z}$, $k \in N$. The local analytic solution for the axisymmetric magnetostatic field problem is the Fourier-Bessel series

$$\begin{aligned} A_\theta = \sum_{k=0}^{\infty} & \left(a_k \cos(\lambda_k z)\mathrm{I}_1(\lambda_k r) + b_k \sin(\lambda_k z)\mathrm{I}_1(\lambda_k r)\right. \\ & \left. + c_k \cos(\lambda_k z)\mathrm{K}_1(\lambda_k r) + d_k \sin(\lambda_k z)\mathrm{K}_1(\lambda_k r)\right) \end{aligned} \tag{10}$$

where a_k, b_k, c_k and d_k depend on the boundary conditions at $r = r_i$ and $r = r_o$.

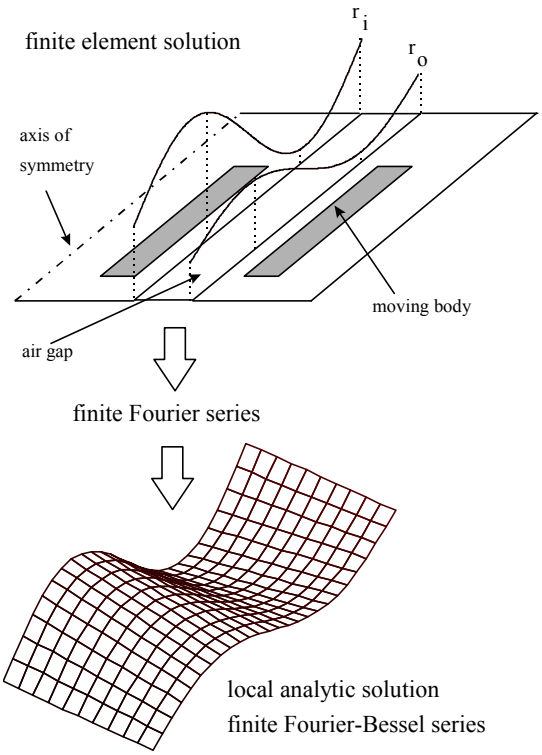

Fig. 3. Algorithm of the enhanced force calculation technique: finite element solution, finite Fourier series and local analytic solution.

7.- FINITE ELEMENT SOLUTION USED AS BOUNDARY CONDITION

Consider a local post-processing domain in the air gap between two moving bodies (fig. 3). The assumption of z-periodicity is valid as long as individual poles of long tubular devices or models with a sufficient amount of surrounding air are concerned (fig. 4). The magnetic vector potential values are extracted out of the finite element solution at the inner and outer boundaries and represented by the n-points Fast Fourier Transforms (FFTs)

$$A_\theta(r_i, z) = \sum_{k=0}^{n} \left(a_{k,i} \cos(\lambda_k z) + b_{k,i} \sin(\lambda_k z)\right) \tag{11}$$

and

$$A_\theta(r_o, z) = \sum_{k=0}^{n} \left(a_{k,o} \cos(\lambda_k z) + b_{k,o} \sin(\lambda_k z)\right) . \tag{12}$$

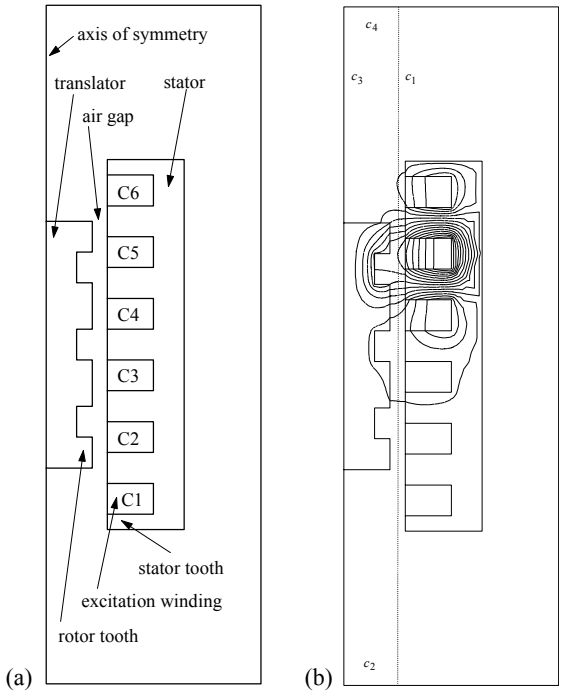

Fig. 4. (a) Outline and (b) flux line plot of the tubular switched reluctance motor.

The approximative local analytic solution is formed by the *n*-terms truncated version of (10) (fig. 3). The coefficients a_k, b_k, c_k and d_k follow from

$$\begin{bmatrix} \mathrm{I}_1(\lambda_k r_i) & \mathrm{K}_1(\lambda_k r_i) \\ \mathrm{I}_1(\lambda_k r_o) & \mathrm{K}_1(\lambda_k r_o) \end{bmatrix} \cdot \begin{bmatrix} a_k \\ c_k \end{bmatrix} = \begin{bmatrix} a_{k,i} \\ a_{k,o} \end{bmatrix}, \; k = 1, \ldots, n \quad (13)$$

and

$$\begin{bmatrix} \mathrm{I}_1(\lambda_k r_i) & \mathrm{K}_1(\lambda_k r_i) \\ \mathrm{I}_1(\lambda_k r_o) & \mathrm{K}_1(\lambda_k r_o) \end{bmatrix} \cdot \begin{bmatrix} b_k \\ d_k \end{bmatrix} = \begin{bmatrix} b_{k,i} \\ b_{k,o} \end{bmatrix}, \; k = 1, \ldots, n \quad (14)$$

It is now possible to derive the magnetic flux density (5) inside the post-processing area from (10) in an analytic way.

$$B_r = \sum_{k=1}^{n} \lambda_k \left(a_k \sin(\lambda_k z) \mathrm{I}_1(\lambda_k r) - b_k \cos(\lambda_k z) \mathrm{I}_1(\lambda_k r) + c_k \sin(\lambda_k z) \mathrm{K}_1(\lambda_k r) - d_k \cos(\lambda_k z) \mathrm{K}_1(\lambda_k r) \right) \quad (15)$$

$$B_z = \sum_{k=1}^{n} \lambda_k \left(a_k \cos(\lambda_k z) \mathrm{I}_0(\lambda_k r) + b_k \sin(\lambda_k z) \mathrm{I}_0(\lambda_k r) - c_k \cos(\lambda_k z) \mathrm{K}_0(\lambda_k r) - d_k \sin(\lambda_k z) \mathrm{K}_0(\lambda_k r) \right) \quad (16)$$

8.- FORCE CALCULATION

The force is computed as an integral of the Maxwell stress tensor along a surface containing the moving part [7]. In axisymmetric models, the force components in the θ-direction and in the *r*-direction vanish. The surface corresponds to a closed contour (c_1-c_4 in fig. 4b). Because of the *z*-periodicity, the contributions to the force of the integrals along the horizontal parts c_2 and c_4 are in opposite and cancel. The integration of the stress tensor along the axis c_3 is zero. Consequently, the force in the *z*-direction is the integral along a line parallel to the axis of symmetry:

$$F_z = \int_{z_1}^{z_2} \nu_0 B_r B_z 2\pi r \, dz \; . \quad (17)$$

The expressions (15) and (16) are substituted in (17). The force in the *z*-direction is obtained by integrating (17) along a line $r = r_m$ parallel to the axis and inside the domain of the analytic solution.

$$F_z = 2\pi r_m \nu_0 \frac{\ell_z}{2} \sum_{k=1}^{n} \left(\lambda_k^2 \left(b_k c_k - a_k d_k \right) \cdot \left(\mathrm{I}_1(\lambda_k r_m) \mathrm{K}_0(\lambda_k r_m) + \mathrm{I}_0(\lambda_k r_m) \mathrm{K}_1(\lambda_k r_m) \right) \right) . \quad (18)$$

The equality $\mathrm{I}_1(t)\mathrm{K}_0(t) + \mathrm{I}_0(t)\mathrm{K}_1(t) = \frac{1}{t}$ [19] is used to reduce (18) to

$$F_z = 2\pi^2 \nu_0 \sum_{k=1}^{n} k \left(b_k c_k - a_k d_k \right) . \quad (19)$$

The force does not depend on the actual chosen contour $r = r_m$. This indicates that the enhanced technique shows in this respect the same characteristic as do commonly used averaging techniques. The fundamental difference is however that the force is obtained directly from the second order convergent potential field instead of from the first order convergent flux densities. A strong resemblance is seen between (19) and the expression derived in an analogue way for the torque in 2D Cartesian models [17].

The computational work and the convergence factor of the enhanced force calculation depends on the number of terms *n* considered in the truncated Fourier-Bessel series. The numerical efforts are mainly determined by the evaluation of the magnetic vector potentials in *2n* points in the post-processing domain and the *4n* Bessel-function evaluations required to compute *n* sets of coefficients a_k, b_k, c_k and d_k.

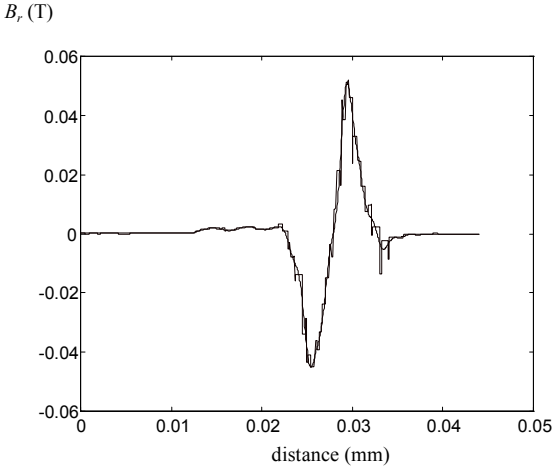

Fig. 5. Magnetic flux density in the *r*-direction: numerical differentiation (solid) versus local post-processing approach (dotted).

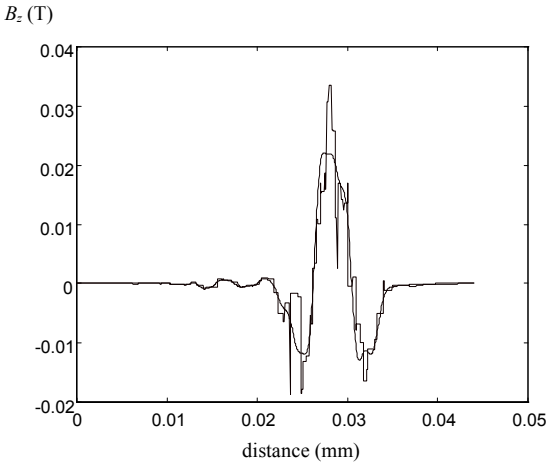

Fig. 6. Magnetic flux density in the *z*-direction: numerical differentiation (solid) versus local post-processing approach (dotted).

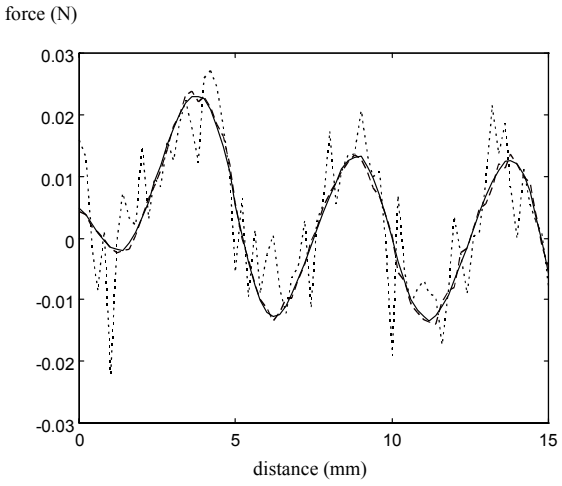

Fig. 7. Dependence of the reluctance force on the position of the translator: Maxwell stress method together with the novel approach (solid line) and virtual work principle (dotted line).

9.- EXAMPLE

Force simulations of a switched reluctance tubular motor [20],[21] with 6 stator slots, 7 stator teeth and 4 rotor teeth are presented (fig. 4a). A first order finite element triangle discretisation is constructed. The solution for the magnetic vector potential is shown in fig. 4b.

A rectangular domain, spanning half of the width of the air gap is used as the local post-processing domain. The 256-points Fourier series of the magnetic vector potential on both sides of the domain form the boundary conditions of the local differential problem. A finite Fourier-Bessel series is constructed. The magnetic flux densities obtained by the enhanced approach is compared to those obtained numerically in fig. 5 and fig. 6. The dependence of the force on the position of the translator is plotted in fig. 7. The convergences of the force errors for the different methods are compared in fig. 8 and Table 1. The convergence rate of the Fourier-Bessel based force computation is higher compared to the classical Maxwell stress approaches, with the averaging of results obtained along 3, 5 and 7 different contours. The convergence rates indicate the theoretical difference of a rate -1 for the enhanced method against the rate -½ for the classical technique when referred to the number of degrees of freedom. The averaging methods do not improve the convergence rate substantially but have an influence on the convergence factor. The scheme with 3 and 5 contours have a decreasing convergence factor. The scheme with 7 contours seems to suffer from the closeness of the stator and rotor teeth.

The technical importance of the improved force computation is the fact that a certain accuracy (e.g. 2 % in fig. 8) is reached with a smaller problem size (600 DOFs instead of 1000 DOFs) or a desired accuracy for the force is attainable within the existing computation resources (e.g. 0.1 % in fig. 8).

10.- CONCLUSIONS

The convergence loss due to the numerical differentiation of the magnetic vector potential in the classical application of the Maxwell stress method, is overcome by employing a local analytic field solution. For axisymmetric models, a finite Fourier-Bessel series is constructed using the finite element solution as the boundary conditions on two sides of the air gap. The force calculation is performed on the series solution. The resulting force retains the same convergence rate as the potential field and does not depend on the mesh orientation and the actual chosen integration contour. The method is applied to a tubular reluctance motor. An extensive comparison is made between the classical Maxwell stress method and the improved force calculation scheme.

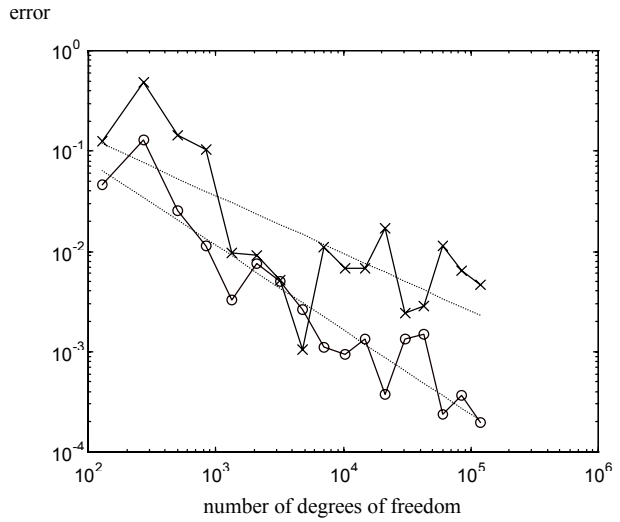

Fig. 8. Convergence of the Fourier-Bessel based force calculation (o) compared to the classical Maxwell stress approach (x).

Table 1: Convergence rate p and convergence factor C

Method	Convergence rate exponent p	Convergence factor C
Maxwell stress	-0.58	6
Maxwell stress (3)	-0.73	8
Maxwell stress (5)	-0.43	0.8
Maxwell stress (7)	-0.65	4
Fourier-Bessel	-0.84	7

Acknowledgment

The authors are grateful to the Belgian "Fonds voor Wetenschappelijk Onderzoek Vlaanderen" for its financial support of this work (project G.0427.98) and the Belgian Ministry of Scientific Research for granting the IUAP No. P4/20 on Coupled Problems in Electromagnetic Systems. The research Council of the K.U.Leuven supports the basic numerical research.

References

[1] Silvester, P.P., Ferrari, R.L., 1996, Finite elements for electrical engineers, 3rd ed., Cambridge University Press, New York, USA.

[2] Binns, K.J., Lawrenson, P.J., Trowbridge, C.W., 1992, The analytical and numerical solution of electric and magnetic fields, Wiley, Chichester, UK.

[3] Pahner, U., Belmans, R., Brandiski, K., Webb, J., Lowther, D., Henrotte, F., Legros, W.: Different formulations in axisymmetric magnetostatic problems, in Nicolet, A., Belmans, R. (eds), 1995, Electric and Magnetic Fields, Plenum Press, New York, USA, pp. 201-204.

[4] Johnson, C., 1987, Numerical solution of partial differential equations by the finite element method, Cambridge University Press, Cambridge, UK.

[5] Hameyer, K., Mertens, R., Pahner, U., Belmans, R., New technique to enhance the accuracy of 2-D/3-D field quantities and forces obtained by standard finite-element solutions, IEE Proc.-Sci. Meas. Technol., Vol. 145, No. 2, 1998, pp. 67-75.

[6] Coulomb, J.L., Meunier, G., Finite element implementation of virtual work principle for magnetic or electric force and torque computation, IEEE Trans. on Magn., Vol. Mag-20, No. 5, 1984, pp. 1894-1896.

[7] DeBortoli, M.J., Salon, S.J., Computation of forces and torques in electromagnetic devices using the finite element method, ICEM90, Vol. 2, 1990, pp. 699-705.

[8] Shi ,Z.W., Rajanathan, C.B., A new method to improve the accuracy of Maxwell stress based force calculation in computational electromagnetic fields, Proc. 3rd Int. Conf. on Computation in Electromagnetics, 1996, pp. 241-246.

[9] Tsukerman, I., Lavers, J.D., Konrad, A., Using complementary formulations for accurate computations of magnetostatic fields and forces in a synchronous motor, IEEE Trans. on Magn., Vol. 30, No. 5, 1994, pp. 3479-3482.

[10] Henneberger, G., Sattler, Ph.K., Shen, D., Force calculation with analytical accuracy in the finite element based computational magnetostatics, IEEE Trans. on Magn., Vol. 27, No. 5, 1991, pp. 4254-4257.

[11] Hamdi, E.S., Licariao-Nogueira, A.F., Silvester, P.P., Torque computation by mean and difference potentials, IEE Proc.-A, Vol. 140, No.2, 1993, pp. 151-154.

[12] Hamler, A., Hribernik, B., Likar, M., Guid, N., Torque calculation by Bernstein Bézier's surfaces, IEEE Trans. on Magn., Vol. 31, No. 3, 1995, pp. 1885-1887.

[13] Trlep, M., Hamler, A., Hribernik, B., Various approaches to torque calculations by FEM and BEM, Proc. 7th Int. IGTE Symp., 1996, pp. 416-419.

[14] Silvester, P.P., Omeragic, D., Differentiation of finite element solutions of the Poisson equation, IEEE Trans. on Magnetics, Vol. 29, No. 2, 1993, pp. 1993-1996.

[15] Kasper, M., Franz, J., Highly accurate computation of field quantities and forces by superconvergence in finite elements, IEEE Trans. on Magnetics, Vol. 31, No. 3, 1995, pp. 1424-1427.

[16] Delaere, K., Belmans, R., Hameyer, K., Vanden Wyngaert, H., Broddin, D., Simulation of toner particle motion under dynamic field conditions in electrostatic printing, Proc. 4th Int. Workshop on Electric and Magnetic Fields, 1998, pp. 529-534.

[17] Mertens, R., Pahner, U., Hameyer, K., Belmans, R., Force calculation based on a local solution of Laplace's equation, IEEE Trans. on Magnetics, Vol. 33, No. 2, 1997, pp. 1216-1218.

[18] Morse, Ph.M., Feshbach, H., 1953, Methods of theoretical physics, McGraw-Hill, New York, USA.

[19] Watson, G.N., 1966, A treatise on the theory of Bessel functions, Cambridge University Press, Cambridge, UK.

[20] Miller, T.J.E., 1989, Brushless permanent-magnet and reluctance motor drives, Clarendon Press, Oxford, UK.

[21] Nasar, S.A., Boldea, I., Unnewehr, L.E., 1993, Permanent magnet, reluctance, and self-synchronous motors, CRC Press, Boca Raton, USA.